

# Toward the Minimal Floating Operation Count Cholesky Decomposition of Electron Repulsion Integrals

Tianyuan Zhang, Xiaolin Liu, Edward F. Valeev, and Xiaosong Li\*



Cite This: *J. Phys. Chem. A* 2021, 125, 4258–4265



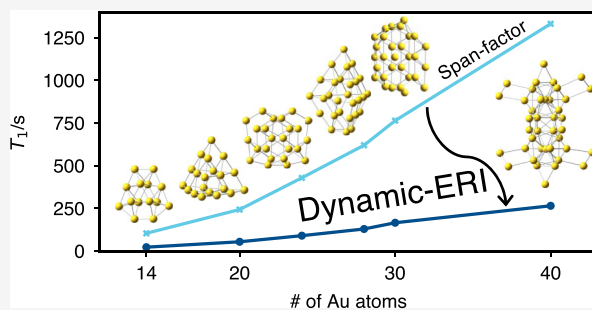
Read Online

ACCESS |

Metrics & More

Article Recommendations

**ABSTRACT:** As quantum chemistry calculations deal with molecular systems of increasing size, the memory requirement to store electron-repulsion integrals (ERIs) greatly outpaces the physical memory available in computing hardware. The Cholesky decomposition of ERIs provides a convenient yet accurate technique to reduce the storage requirement of integrals. Recent developments of a two-step algorithm have drastically reduced the memory operation (MOP) count, leaving the floating operation (FLOP) count as the last frontier of cost reduction in the Cholesky ERI algorithm. In this report, we introduce a dynamic integral tracking, reusing, and compression/elimination protocol embedded in the two-step Cholesky ERI method. Benchmark studies suggest that this technique becomes particularly advantageous when the basis set consists of many computationally expensive high-angular-momentum basis functions. With this dynamic-ERI improvement, the Cholesky ERI approach proves to be a highly efficient algorithm with minimal FLOP and MOP count.



## 1. INTRODUCTION

Quantum chemistry calculations using localized atomic orbitals require the computation of four-index electron-repulsion integrals (ERIs) which scales as  $\mathcal{M}(N^4)$  in memory storage requirement for the in-core tensor product, where  $N$  is the number of basis functions. The memory requirement for storing ERIs can be reduced by using the Cholesky decomposition (CD)<sup>1–6</sup> or the resolution-of-the-identity (RI)<sup>7–9</sup> techniques to approximate the four-index ERI tensor as a product of two three-index tensors.<sup>10–21</sup> The main difference between the RI and CD techniques is that the former requires a preoptimized auxiliary basis set, whereas the latter constructs it on-the-fly. Being able to work with general basis sets and elements gives the Cholesky ERI approach a practical advantage over RI. Additionally, the CD method features a tunable accuracy and is generally more accurate than the RI method when their three-index tensors have similar sizes.<sup>22</sup> However, the computational cost of the conventional algorithm to build the CD three-index tensor is drastically greater than RI. This is mainly due to the need to determine the Cholesky pivot set, which is the analogue of the auxiliary basis set in RI.

In the conventional CD method, when a pair of basis functions is selected as a pivot (Cholesky basis), all associated ERI elements are evaluated for the construction of the Cholesky vectors.<sup>3</sup> However, the conventional algorithm discards many of the evaluated elements that are potentially useful in future iterations. This is because there is no easy way

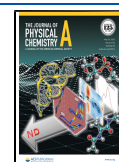
to predict which ERI elements in a shell quartet are needed in future iterations, and storing all of them is not practical. This situation becomes more severe when the system includes many high-angular-momentum basis shells. In this case, construction of each new Cholesky vector requires looping over all previous Cholesky vectors with length  $N^2$ . When the number of selected Cholesky pivots is great, the processing speed is limited by the memory bandwidth and memory operation (MOP) count.

To mitigate this issue, Aquilante and co-workers proposed a two-step framework as an alternative to the conventional CD method.<sup>23</sup> The two-step algorithm splits the task into the prediction and construction steps: (1) determine the Cholesky pivots and (2) build the 3-index ERI tensors. In this way, the second step is similar to the RI algorithm, where all necessary ERI elements are evaluated only once and the three-index tensor is built directly by matrix multiplication with an optimal memory bandwidth requirement. Meanwhile, in the first step, since only the diagonal elements need to be evaluated and the exact three-index vectors are not computed, elements connected to unimportant basis pairs can be discarded. This fact is utilized in the span-factor algorithm proposed along with

**Received:** March 15, 2021

**Revised:** April 21, 2021

**Published:** May 10, 2021



the two-step framework, which was recently improved by Folkestad and co-workers,<sup>24</sup> which determines the Cholesky pivots in batches. As a result, the overall cost is only a fraction of the conventional algorithm. The span-factor algorithm successfully resolves the memory bottleneck issue in the Cholesky ERI algorithm, but the costly high-angular-momentum shell quartets are still evaluated multiple times. In this work, we continue to improve the efficiency of the two-step Cholesky ERI algorithm by introducing a dynamic ERI tracking, reusing, and compression/elimination protocol when determining the Cholesky pivot set. With this dynamic-ERI improvement, the Cholesky ERI approach can be shown to be a highly efficient algorithm with minimal floating operation (FLOP) count and an optimal MOP count, supported by benchmark studies.

## 2. METHODS

We use the following notations throughout this work:

- $A, B, C, D, \dots$  are basis shells;
- $P, Q, R, S, \dots$  are basis shell pairs;
- $\mu, \nu, \lambda, \gamma, \dots$  are basis functions;
- $p, q, r, s, t, u, \dots$  are basis function pairs;
- $L^p$  is the Cholesky vector for the pivot basis function pair  $p$ ;
- Calligraphic notations ( $\mathcal{B}, \mathcal{L}, \mathcal{P}, \mathcal{Q}, \dots$ ) are sets/containers, and their cardinalities are labeled by  $|\mathcal{B}|, |\mathcal{L}|, |\mathcal{P}|, |\mathcal{Q}|, \dots$ ;
- Set/container insert, union, and minus are represented by operators  $\rightarrow, \cup$ , and  $\setminus$ , respectively;
- $\text{Diag}(r)$  is the diagonal element associated with  $r$  in the CD algorithm;
- $i$  is the index for outer iteration, and  $j$  is the index for inner iteration.

**2.1. Conventional Algorithm.** The four-index ERI tensor over basis functions in the chemist (Mulliken) notation ( $\mu\nu\lambda\gamma$ ) can be cast as a two-index matrix  $M_{rs} = (r|s)$ , where  $\mu, \nu, \lambda, \gamma$  are basis functions,  $r \equiv \mu\nu$  and  $s \equiv \lambda\gamma$  are basis function pairs. Due to the nature of electron repulsion, such an ERI matrix is positive semidefinite and can be Cholesky-decomposed to a product of a lower triangular matrix ( $L$ ) and its transpose

$$(\mu\nu\lambda\gamma) \equiv M_{rs} = \sum_p L_r^p L_s^p = (LL^T)_{rs} \quad (1)$$

where  $L^p$  are Cholesky (column) vectors in  $L$ . In the exact CD, since the dimension of  $L$  is  $(N^2 \times N^2)$ , where  $N$  is the number of basis functions, there is no computational saving in either memory storage or floating point operations (FLOPs).

The Cholesky ERI algorithm aims to directly construct a set of Cholesky vectors with a reduced length that can produce ERIs within a tolerance or accuracy threshold

$$(\mu\nu\lambda\gamma) \equiv M_{rs} \approx \sum_{p \in \mathcal{B}} L_r^p L_s^p \quad (2)$$

where  $\mathcal{B}$  is the set of basis pairs selected as Cholesky bases (pivots). Usually, the length of  $\mathcal{B}$  is much smaller than  $N^2$  ( $|\mathcal{B}| \ll N^2$ ), leading to significant savings in the ERI storage.

The conventional Cholesky ERI algorithm iteratively adds new basis pairs into the Cholesky pivot set  $\mathcal{B}$  based on a selection criterion, which usually corresponds to the largest diagonal ERI remaining in  $\text{Diag}(r)|_{r \notin \mathcal{B}}$ . The iteration starts

with precomputed diagonal elements of ERIs,  $\text{Diag}(r) = (r|r) \equiv (\mu\nu|\mu\nu)$ .

When a basis pair  $q$  that satisfies  $\text{Diag}(q) = \max[\text{Diag}(r)|_{r \notin \mathcal{B}}]$  is selected as the new pivot, a new Cholesky vector  $L^q$  can be generated as

$$L_s^q = \begin{cases} \frac{(q|s) - \sum_{p \in \mathcal{B}} L_q^p L_s^p}{\sqrt{\text{Diag}(q)}} & \text{for } \text{Diag}(q) > 0, \\ 0 & \text{otherwise,} \end{cases} \quad \text{for } s \notin \mathcal{B} \quad (3)$$

$$L_s^q = 0, \quad \text{for } s \in \mathcal{B} \quad (4)$$

$q$  is then added to the Cholesky pivot set  $\mathcal{B}$ . The total computational cost for generating Cholesky vectors using eq 3 is  $O(|\mathcal{B}|^2 N^2)$  in FLOP and  $M(|\mathcal{B}|^2 N^2)$  in MOP counts.

When the new basis pair  $q$  is moved to the Cholesky pivot set, the  $\text{Diag}(r)$  values are updated as

$$\text{Diag}(r) = \text{Diag}(r) - (L_r^q)^2 \quad (5)$$

in order to evaluate the importance of the remaining basis pairs. A new iteration starts with the updated  $\text{Diag}(r)$ . In the conventional Cholesky ERI approach, when  $\text{Diag}(r) < \tau_0$  for all  $r \notin \mathcal{B}$ , the remaining basis pairs are considered insignificant and the iteration stops.

If we use  $\tilde{M}$  to represent the difference between the exact matrix  $M$  and  $LL^T$

$$\tilde{M} = M - LL^T \quad (6)$$

the diagonal elements of  $\tilde{M}$  are

$$\tilde{M}_{rr} = \text{Diag}(r) \quad (7)$$

According to the Cauchy–Schwarz inequality

$$\tilde{M}_{rs}^2 \leq \tilde{M}_{rr} \tilde{M}_{ss} \leq \tau_0^2 \quad (8)$$

the error in approximation

$$(\mu\nu\lambda\gamma) \equiv (r|s) \approx \sum_{p \in \mathcal{B}} L_r^p L_s^p \leq \tau_0 \quad (9)$$

for all ERI elements.

The conventional Cholesky ERI approach approximates  $O(N^4)$  ERI elements using three-index tensors of size  $O(|\mathcal{B}|N^2)$ , where  $|\mathcal{B}|$  is the number of Cholesky basis. The accuracy and  $|\mathcal{B}|$  is controlled by a single threshold  $\tau_0$ . However, the procedure to generate Cholesky vectors (eq 3) can be computationally expensive as all vectors of length  $N^2$  have to be looped over.

**2.2. Two-Step Algorithm.** Alternatively, Cholesky vectors can be formed through a two-step algorithm.<sup>23</sup> The idea behind the two-step algorithm is similar to RI using an auxiliary basis, except that in this case, the auxiliary basis is the set of Cholesky pivots.

In the first step, a procedure similar to the conventional approach is used to determine the set of Cholesky basis (pivots)  $\mathcal{B}$  without computing the complete Cholesky vectors.

In the second step, an RI-like algorithm is used. A matrix  $J$  can be computed with elements

$$J_{pp'} = (p|p'), \quad p, p' \in \mathcal{B} \quad (10)$$

The ERI approximation in eq 9 can be equivalently written in an inner projection form

**Algorithm 1:** Cholesky Pivot Determination

---

```

1 Initialize a list  $\mathcal{B}$  to store selected Cholesky pivots;
2 Initialize a container  $\mathcal{L}$  to store computed Cholesky vectors;
3 Initialize a container  $\mathcal{E}$  to store computed ERIs;
4 Initialize a container  $\mathcal{P}$  to store Cholesky pivot candidates;
5 for  $R = AB, A \leq B$  do
6   Compute diagonal shell quartet  $(R|R)$ ;
7   for  $r \in R$  &  $\text{Diag}(r) \equiv (r|r) \geq \tau_0$  do  $r \rightarrow \mathcal{P}_R$ ;
8   for  $r, s \in \mathcal{P}_R$  do  $(r|s) \rightarrow \mathcal{E}$ ;
9    $\mathcal{P} = \mathcal{P} \cup \mathcal{P}_R$ ;
10 end
11 while  $|\mathcal{P}| \neq 0$  do
12    $D_{\max} = \max_{r \in \mathcal{P}} \text{Diag}(r)$ ;
13   Select  $\text{Diag}(r)|_{r \in \mathcal{P}} \geq \sigma D_{\max}$  where  $\sigma$  is the “span factor”;
14   if  $|\{r\}| > m_\sigma$  then Only select the largest  $m_\sigma$  number of  $\text{Diag}(r)|_{r \in \mathcal{P}}$ ;
15   Initialize an empty container  $\mathcal{Q}$ , store selected  $\{r\}$  in  $\mathcal{Q}$ ;
16   for  $s \in \mathcal{Q}$  do
17     for  $r \in \mathcal{P}$  do
18       if  $(r|s) \notin \mathcal{E}$  then
19         Compute shell quartet  $(R|S)$ , where  $r \in R$  and  $s \in S$ ;
20         for  $t \in R, u \in S$  &  $t, u \in \mathcal{P}$  do  $(t|u) \rightarrow \mathcal{E}, (u|t) \rightarrow \mathcal{E}$ ;
21       end
22        $\widetilde{M}_{rs} = (r|s) - \sum_{L^p \in \mathcal{L}} L_r^p L_s^p$ ;
23     end
24   end
25   if  $\mathcal{P} \setminus \mathcal{Q} \neq 0$  then  $\tau = \max_{r \in \mathcal{P} \setminus \mathcal{Q}} \text{Diag}(r)$ ;
26   else  $\tau = \tau_0$ ;
27   while  $\mathcal{Q} \neq 0$  &  $\text{Diag}(q) = \max_{r \in \mathcal{Q}} \text{Diag}(r)$  &  $\text{Diag}(q) \geq \tau$  do
28     Initialize a container  $\mathcal{L}^{(i)}$  to store new Cholesky vectors;
29     for  $r \in \mathcal{P}$  do
30        $L_r^q = \frac{\widetilde{M}_{rq} - \sum_{L^p \in \mathcal{L}^{(i)}} L_r^p L_q^p}{\sqrt{\text{Diag}(q)}}$ ;
31        $\text{Diag}(r) = \text{Diag}(r) - (L_r^q)^2$ ;
32     end
33      $\mathcal{Q} = \mathcal{Q} \setminus \{q\}, q \rightarrow \mathcal{B}, L^q \rightarrow \mathcal{L}^{(i)}$ ;
34   end
35    $\mathcal{L} = \mathcal{L} \cup \mathcal{L}^{(i)}$ ;
36   for  $r \in \mathcal{P}$  do
37     if  $\text{Diag}(r) < \tau$  then
38       for  $s \in \mathcal{P}$  do  $\mathcal{E} = \mathcal{E} \setminus \{(r|s)\}, \mathcal{E} = \mathcal{E} \setminus \{(s|r)\}$ ;
39       Compress the length of  $L \in \mathcal{L}$  by removing the element  $r$ ;
40     end
41   end
42 end

```

---

$$(\mu\nu|\lambda\gamma) \approx \sum_{p,p' \in \mathcal{B}} (\mu\nu|p')(\mathbf{J}^{-1})_{p'p}(p|\lambda\gamma) \quad (11)$$

By Cholesky-decomposing  $\mathbf{J} = \mathbf{K}\mathbf{K}^T$ , the Cholesky vectors in eq 9 can be easily formed

$$L_{\mu\nu}^p = \sum_{p' \in \mathcal{B}} (\mu\nu|p')(\mathbf{K}^{-T})_{p'p} \quad (12)$$

where  $\mathbf{K}^{-T} \equiv (\mathbf{K}^T)^{-1}$ .

There are several clear advantages of the two-step Cholesky ERI algorithm over the conventional approach. After determining the Cholesky pivot set  $\mathcal{B}$  and its associated Coulomb matrix  $\mathbf{J}$ , the procedures to construct Cholesky vectors can take advantage of high-performance BLAS and LAPACK libraries, including the CD of  $\mathbf{J}$ , the inversion of the triangular matrix  $\mathbf{K}^T$ , and the contraction between the three-index ERI tensor  $(\alpha\beta|p')$  and  $\mathbf{K}^{-T}$ . The FLOP count in the linear algebra portion of the conventional algorithm (eq 3) is comparable to the cost of eq 12; both scale as  $O(|\mathcal{B}|^2 N^2)$ . However, the MOP count is higher in the conventional

method compared to the two-step approach, that is,  $M(|\mathcal{B}|^2 N^2)$  versus  $M(|\mathcal{B}|N^2)$ , respectively. Additionally, in the conventional approach, there is no mechanism to reuse integrals that are previously computed, and, as a result, there are many redundant integral evaluations. In contrast, in the two-step approach, the redundancy in integral evaluation can be completely eliminated in eq 12, given the set of known Cholesky bases obtained in the first step.

Unlike the relative straightforward implementation of the conventional Cholesky ERI approach, in order for the two-step method to reach its full potential, several important cost-reduction techniques and considerations must be employed. The key lies in an efficient way to determine the Cholesky pivot set without computing all Cholesky vectors in the first step.

**2.3. Efficient Cholesky Pivot Determination.** Recently, Folkestad and co-workers proposed the so-called “span-factor” algorithm to efficiently determine the Cholesky pivot set.<sup>24</sup> Here, we introduce a new algorithm that features a reduced FLOP count by avoiding redundant evaluations of the basis

**Table 1. Computational Costs (in Seconds) of Computing Cholesky Vectors Using the Conventional, Span-Factor, and Dynamic-ERI Approaches<sup>a</sup>**

method	$T_1$				$T_2$			total
	$N_{1,\text{SQ}}$	$T_{1,\text{ERI}}$	$T_{1,\text{CD}}$	$T_{1,\text{COM}}$	$N_{2,\text{SQ}}$	$T_{2,\text{ERI}}$	$T_{2,\text{MM}}$	
$\tau_0 = 1 \times 10^{-4b}$								
conventional	$1.85 \times 10^9$	285.3	504.7					801.0
span-factor	$1.12 \times 10^8$	16.0	3.8	0.2	$1.85 \times 10^9$	286.0	14.4	327.2
dynamic-ERI	$7.00 \times 10^7$	9.7	3.8	0.2	$1.85 \times 10^9$	287.2	14.1	322.1
$\tau_0 = 1 \times 10^{-6c}$								
sonventional	$4.59 \times 10^9$	701.5	3086.4					3823.5
span-factor	$5.61 \times 10^8$	81.0	12.1	1.3	$4.55 \times 10^9$	721.9	86.1	918.5
dynamic-ERI	$2.67 \times 10^8$	38.0	12.7	1.9	$4.55 \times 10^9$	721.2	85.5	876.0
$\tau_0 = 1 \times 10^{-8d}$								
conventional	$7.11 \times 10^9$	1092.3	7112.2					8259.5
span-factor	$1.71 \times 10^9$	248.4	36.9	5.1	$7.01 \times 10^9$	1119.8	206.3	1649.0
dynamic-ERI	$6.72 \times 10^8$	96.1	39.2	8.3	$7.01 \times 10^9$	1113.8	202.7	1492.1

<sup>a</sup>This system consists of  $10 \times 10 \times 10$  H atoms in a cube. The distance between adjacent H atoms is 1.0 Å. The STO-3G<sup>27</sup> (1000 basis functions) is used in this test. Note that the storage requirement for the full four-index ERI tensor is 8 TB. The reference Hartree–Fock energy using AO-direct four-index ERI is  $-388.14611071$  au. <sup>b</sup>Three-index tensor size = 29.6 GB,  $|B| = 3700$ , initial  $|P| = 43,144$ ,  $\Delta E = 4.4 \times 10^{-1}$  au. <sup>c</sup>Three-index tensor size = 73.3 GB,  $|B| = 9168$ , initial  $|P| = 80,172$ ,  $\Delta E = 1.9 \times 10^{-3}$  au. <sup>d</sup>Three-index tensor size = 113.6 GB,  $|B| = 14,205$ , initial  $|P| = 126,924$ ,  $\Delta E = 4.0 \times 10^{-6}$  au.

**Table 2. Computational Costs (in Seconds) of Computing Cholesky Vectors Using the Conventional, Span-Factor, and Dynamic-ERI Approaches<sup>a</sup>**

method	$T_1$				$T_2$			total
	$N_{1,\text{SQ}}$	$T_{1,\text{ERI}}$	$T_{1,\text{CD}}$	$T_{1,\text{COM}}$	$N_{2,\text{SQ}}$	$T_{2,\text{ERI}}$	$T_{2,\text{MM}}$	
$\tau_0 = 1 \times 10^{-4b}$								
conventional	$2.47 \times 10^8$	104.3	354.5					468.4
span-factor	$2.31 \times 10^7$	8.6	2.5	0.9	$4.60 \times 10^7$	30.5	9.9	57.1
dynamic-ERI	$1.06 \times 10^7$	4.2	2.2	0.6	$4.60 \times 10^7$	30.7	10.2	53.0
$\tau_0 = 1 \times 10^{-6c}$								
traditional	$4.33 \times 10^8$	155.0	1114.9					1286.5
span-factor	$6.91 \times 10^7$	19.5	19.8	4.8	$8.56 \times 10^7$	43.9	31.3	129.5
dynamic-ERI	$1.97 \times 10^7$	7.4	11.4	3.3	$8.56 \times 10^7$	44.2	31.0	107.1
$\tau_0 = 1 \times 10^{-8d}$								
conventional	$7.22 \times 10^8$	263.2	3222.1					3517.7
span-factor	$1.64 \times 10^8$	39.8	95.9	23.9	$1.58 \times 10^8$	68.7	86.9	331.5
dynamic-ERI	$3.67 \times 10^7$	11.3	33.4	9.9	$1.58 \times 10^8$	68.1	89.6	230.1

<sup>a</sup>A  $\text{C}_{60}$  molecule with the cc-pVDZ<sup>28</sup> basis set (840 basis functions) is used in this test. Note that the storage requirement for the full four-index ERI tensor is 4 TB. The reference B3LYP<sup>29–31</sup> energy using AO-direct four-index ERI is  $-2286.08361884$  au. <sup>b</sup>Three-index tensor size = 21 GB,  $|B| = 3802$ , initial  $|P| = 58,923$ ,  $\Delta E = 1.0 \times 10^{-3}$  au. <sup>c</sup>Three-index tensor size = 38 GB,  $|B| = 6663$ , initial  $|P| = 93,636$ ,  $\Delta E = 4.8 \times 10^{-5}$  au. <sup>d</sup>Three-index tensor size = 63 GB,  $|B| = 11,108$ , initial  $|P| = 123,200$ ,  $\Delta E = 1.7 \times 10^{-7}$  au.

shell quartet. Due to the dynamic nature of ERI tracking and compression in this algorithm, we term it the “dynamic-ERI” algorithm. Both “span-factor” and “dynamic-ERI” algorithms can be organized into algorithm 1.

The idea behind the “span-factor” approach is to determine new Cholesky pivots in batches (lines 12–14 in algorithm 1) so as to take advantage of the fast linear algebra libraries (line 22 in algorithm 1). The size of each candidate batch is controlled by a span factor  $\sigma$  and a maximum qualification number  $m_\sigma$  so that the batch is neither too small to benefit from linear algebra libraries nor too large to minimize the evaluation of unimportant ERI elements. In this paper, we set  $\sigma = 1 \times 10^{-2}$  and  $m_\sigma = 1000$ , as suggested in ref 24. Our preliminary tests show that the efficiency of the algorithm is not sensitive to batch sizes. Detailed investigation will be discussed in a future report.

In the “dynamic-ERI” algorithm, in addition to batching evaluations of Cholesky pivots, all ERIs computed inside the

loop are saved (lines 8 and 20 in algorithm 1) and reused (line 22 in algorithm 1). Due to the fast growing number of ERIs, all integrals are tracked and removed when the associated diagonal elements fall below the threshold (line 39 in algorithm 1). Note that although Cholesky pivots are selected based on basis pairs, efficient ERI evaluations are batched by the shell quartet. As a result, ERI tracking and removal should be carried out in shell pairs.

### 3. BENCHMARKS AND DISCUSSION

The conventional, span-factor, and dynamic-ERI are implemented in the open-source Chronus Quantum package,<sup>25</sup> which uses the LIBINT library<sup>26</sup> for ERI evaluations. Tables 1–3 report timing comparisons of the three Cholesky ERI approaches discussed here. Unless otherwise noted, all computations were performed with 28 threads on a computation node with two Intel Xeon E5-2680 v4 CPUs. Additionally, Chronus Quantum was compiled using the Intel



**Table 3. Computational Costs (in seconds) of Computing Cholesky Vectors Using the Conventional, Span-Factor, and Dynamic-ERI Approaches<sup>a</sup>**

method	$T_1$				$T_2$			total
	$N_{1,\text{SQ}}$	$T_{1,\text{ERI}}$	$T_{1,\text{CD}}$	$T_{1,\text{COM}}$	$N_{2,\text{SQ}}$	$T_{2,\text{ERI}}$	$T_{2,\text{MM}}$	
$\tau_0 = 1 \times 10^{-4b}$								
conventional	$3.64 \times 10^8$	1515.1	1869.0					3415.5
span-factor	$1.87 \times 10^7$	155.4	16.2	3.7	$4.51 \times 10^7$	115.4	55.7	361.1
dynamic-ERI	$6.15 \times 10^6$	13.0	4.6	2.6	$4.51 \times 10^7$	114.5	54.5	204.6
$\tau_0 = 1 \times 10^{-6c}$								
conventional	$5.05 \times 10^8$	1977.2	3608.1					5630.2
span-factor	$4.43 \times 10^7$	277.6	51.5	10.7	$6.56 \times 10^7$	133.6	111.8	609.5
dynamic-ERI	$1.16 \times 10^7$	17.1	16.3	6.5	$6.56 \times 10^7$	133.8	112.2	311.4
$\tau_0 = 1 \times 10^{-8d}$								
conventional	$7.32 \times 10^8$	2681.7	7705.5					10,447.0
span-factor	$8.46 \times 10^7$	459.6	152.4	28.4	$9.49 \times 10^7$	171.4	228.6	1082.8
dynamic-ERI	$1.83 \times 10^7$	21.6	41.3	14.2	$9.49 \times 10^7$	170.3	233.4	525.9

<sup>a</sup>Au<sub>14</sub> cluster with the Jorge-TZP-DKH<sup>32</sup> basis set (1148 basis functions) is used in this test. Note that the storage requirement for the full four-index ERI tensor is 14 TB. The reference ALH-X2C-PBE0<sup>33–44</sup> energy using AO-direct four-index ERI is  $-265,731.11806264$  au. <sup>b</sup>Three-index tensor size = 68 GB,  $|B| = 6436$ , initial  $|P| = 58,377$ ,  $\Delta E = 3.4 \times 10^{-3}$  au. <sup>c</sup>Three-index tensor size = 94 GB,  $|B| = 8920$ , initial  $|P| = 95,009$ ,  $\Delta E = 2.8 \times 10^{-4}$  au. <sup>d</sup>Three-index tensor size = 136 GB,  $|B| = 12,925$ , initial  $|P| = 125,694$ ,  $\Delta E = 2.7 \times 10^{-6}$  au.

C++ Compiler version 19.0.0.117. For the two-step algorithms, we report the time spent to determine the Cholesky pivot set as  $T_1$  and the time to build three-index RI-ERI tensors as  $T_2$  in wall-clock times. The most time-consuming procedures in  $T_1$  include the evaluation of ERI vectors ( $T_{1,\text{ERI}}$ ), the computation of Cholesky vectors ( $T_{1,\text{CD}}$ ), and the compression of Cholesky vectors ( $T_{1,\text{COM}}$ ). For the dynamic-ERI algorithm, we also include the integral tracking and removal time as part of the compression step ( $T_{1,\text{COM}}$ ).  $T_2$  primarily consists of the time to compute three-index ERI elements ( $T_{2,\text{ERI}}$ ) and the matrix multiplication in eq 12 ( $T_{2,\text{MM}}$ ). We also report the total number of shell quartets ( $N_{1,\text{SQ}}$  and  $N_{2,\text{SQ}}$ ) computed during  $T_1$  and  $T_2$ . The conventional algorithm is a single-step approach, which requires the evaluation of ERI vectors ( $T_{\text{ERI}}$ ) and CD ( $T_{\text{CD}}$ ). For convenience, these values are listed together with those in the first step of two-step algorithms.

In Tables 1–3, the computational costs of computing Cholesky vectors are presented for a cubic H<sub>1000</sub> system, a C<sub>60</sub> molecule, and a Au<sub>14</sub> cluster. All three methods result in the same set of Cholesky vectors and identically converged energies for a given threshold  $\tau_0$ .

Both the span-factor and dynamic-ERI algorithms are significantly faster than the conventional Cholesky ERI approach. For the case of H<sub>1000</sub>, since all basis shells are S shells and the conventional method does not repeat evaluation of any shell quartet, the only computational saving in the span-factor and dynamic-ERI algorithms comes from the utilization of the fast linear algebra library to construct the Cholesky vectors ( $T_{2,\text{MM}}$  in span-factor and dynamic-ERI methods versus  $T_{1,\text{CD}}$  in the conventional method). As a result, we only observed a 2.5× speed-up when a loose threshold ( $\tau_0 = 1 \times 10^{-4}$ ) was used. As the threshold is decreased and the size of the Cholesky vectors increases, the advantage of using a fast linear algebra library to construct the Cholesky vector becomes more prominent. At  $\tau_0 = 1 \times 10^{-8}$ , the span-factor and dynamic-ERI methods show a factor of  $\sim 5.5$  speed-up compared to the conventional method. This behavior is consistent throughout the tests carried out here.

For the C<sub>60</sub> and Au<sub>14</sub> test cases, additional computational savings arise from the reduction of the number of shell quartets

evaluated in the Cholesky ERI procedures ( $N_{2,\text{SQ}}$  in span-factor and dynamic-ERI methods versus  $N_{1,\text{SQ}}$  in the conventional approach). The reduced computation in ERI evaluation and the utilization of the fast linear algebra in the span-factor and dynamic-ERI algorithms give rise to a 10–20-fold speed-up for Au<sub>14</sub> with  $\tau_0 = 1 \times 10^{-8}$ .

Comparing the two two-step Cholesky ERI methods, the dynamic-ERI algorithm consistently outperforms the span-factor approach with a speed-up ranging from a factor of 1.02 (H<sub>1000</sub>,  $\tau_0 = 1 \times 10^{-4}$ ) to 2.06 (Au<sub>14</sub>,  $\tau_0 = 1 \times 10^{-8}$ ). The computational savings in the dynamic-ERI algorithm mainly comes from the elimination of redundant ERI evaluations through a tracking and removal process without exhausting the memory resources. For basis sets mostly consisting of low angular momentum functions (i.e., the STO-3G basis set used with H<sub>1000</sub>) the speed-up in the dynamic-ERI algorithm is only marginal (around 10% faster) compared to the span-factor method. As more high-angular-momentum bases are included in the basis set, the computational saving in the dynamic-ERI algorithm becomes more significant. Since both the dynamic-ERI and span-factor algorithms have identical procedures in the second step, the difference in computational savings comes exclusively from the first step. Figure 1 plots ERI efficiencies as a function of average angular momentum of the basis set, including the number of evaluated shell quartets and the time spent on the ERI evaluation. Since the computational cost of ERI evaluation in  $T_2$  can be considered as the theoretical limit when all Cholesky pivots have been determined, the ERI efficiency in each algorithm is defined as the total number of ERI computed and total ERI time relative to  $T_2$ , for example,  $(N_{1,\text{SQ}} + N_{2,\text{SQ}})/N_{2,\text{SQ}}$  and  $(T_{1,\text{ERI}} + T_{2,\text{ERI}})/T_{2,\text{ERI}}$ . Figure 1 shows that the dynamic-ERI algorithm recomputes only 10–20% more ERIs than what is needed for constructing Cholesky vectors. In contrast, the span-factor approach needs to recompute 70–80% more ERIs than those needed in  $T_2$ . If the extra ERIs are associated with high angular momentum bases with high computational cost, the computational saving in the dynamic-ERI algorithm can be significant, as shown for the case of Au<sub>14</sub>.

Figure 2 plots wall-clock times for a series of Au<sub>n</sub> clusters. Across the series, the dynamic-ERI algorithm constantly shows

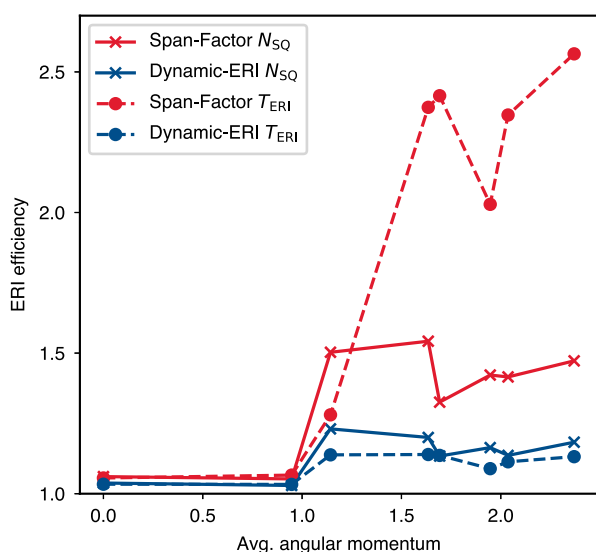


**Figure 1.** ERI efficiency as a function of the average angular momentum of basis. Systems used in this plot are  $H_{1000}$  with STO-3G,<sup>27</sup>  $(H_2O)_{50}$  with 6-31G(d),<sup>45–47</sup>  $C_{60}$  with cc-pVDZ,<sup>28</sup> and  $Au_{14}$  with Jorge-DZP-DKH,<sup>48</sup> Jorge-TZP-DKH,<sup>32</sup> and Sapporo-DKH3-XZP ( $X = D, T, Q$ )<sup>49</sup> at  $\tau_0 = 1 \times 10^{-4}$ . The baseline  $N_{SQ}$  and  $T_{ERI}$  is defined to be  $N_{2,SQ}$  and  $T_{2,ERI}$  of the two-step algorithm. This plot computes the ratio of  $N_{1,SQ} + N_{2,SQ}$  and  $T_{1,ERI} + T_{2,ERI}$  to the baseline.

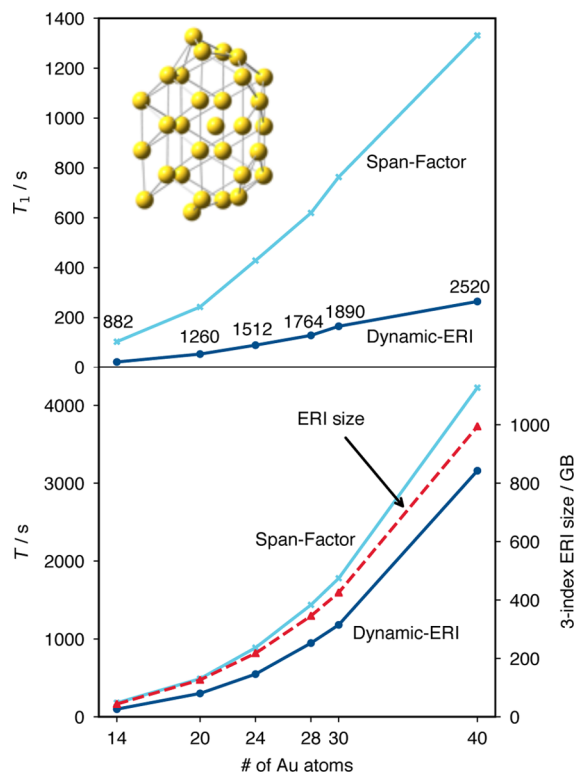


**Figure 2.** (Top) The computational times of Cholesky basis determination (first step). The number of basis functions in each system is labeled along the curve. (Bottom) The computational times of ERI CD and the sizes of result of three-index tensors for gold cluster series of 14, 20, 24, 28, 30, and 40 gold atoms in Jorge-DZP-DKH<sup>48</sup> basis set with  $\tau_0 = 1 \times 10^{-6}$ . Computations were performed with 48 threads on a computation node with two Intel Xeon Platinum 8160M CPUs. Additionally, Chronus Quantum was compiled using the Intel C++ Compiler version 2021.1 Beta 20201112.

an 80% savings in the computational cost to determine Cholesky pivots. However, as the size of the system increases, the second step to build three-index Cholesky tensors dominates the Cholesky ERI procedure. As a result, the dynamic-ERI algorithm shows a 45% computational saving in the overall wall-clock time at  $Au_{14}$  but only 25% at  $Au_{40}$ . Note that storing all three-index Cholesky vectors requires  $\sim 1$  TB memory for 2520 basis functions ( $Au_{40}$ ). As the size of the system increases, the AO-direct algorithm will be a better choice.

Figure 3 shows the parallel performance of the dynamic-ERI algorithm. As expected, the matrix product step ( $T_2$ ), by taking

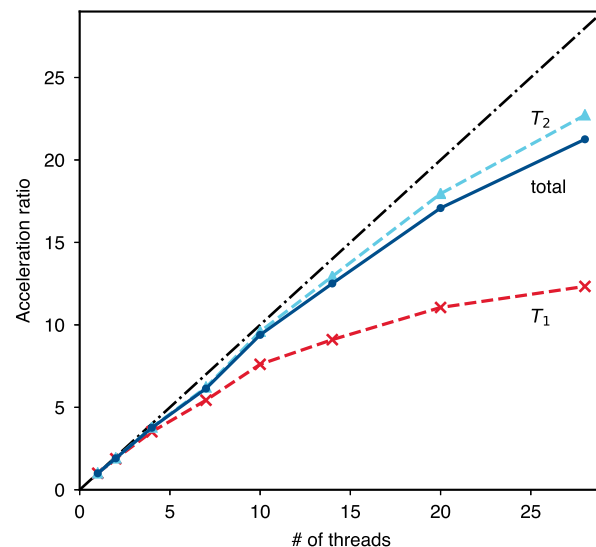


**Figure 3.** Shared-memory parallel acceleration of the dynamic-ERI algorithm in computing the Cholesky vectors of the  $Au_{14}$  cluster using the Jorge-TZP-DKH<sup>32</sup> basis set (1148 basis functions) with  $\tau_0 = 1 \times 10^{-6}$ . We show the acceleration ratio,  $T(1 - \text{core})/T(n - \text{core})$ , in the first step, second step, and total time.

advantage of linear algebra libraries, nicely scales with respect to the number of computing cores. Since not all procedures in the first step ( $T_1$ ) can be vectorized, its parallel performance is not ideal. However, since the computational cost of  $T_1$  is only a small fraction of that of  $T_2$ , the overall parallel performance of the dynamic-ERI algorithm is still near optimal.

#### 4. CONCLUSIONS

In this work, we introduced an efficiency-improved two-step Cholesky ERI method. The algorithm focuses on minimizing the FLOP count in the ERI evaluation by employing an ERI tracking, reusing, and eliminating protocol without exhausting the memory resource. Benchmark tests show that the dynamic-ERI algorithm consistently outperforms the span-factor approach, with both methods being significantly faster than the conventional Cholesky ERI method. The advantage of the dynamic-ERI algorithm becomes more prominent as more high angular momentum bases are used. We also demonstrated the excellent parallel scaling of the dynamic-ERI method as the underlying algorithm is designed to take the full advantage of linear algebra libraries in both steps.

## ■ AUTHOR INFORMATION

## Corresponding Author

Xiaosong Li – Department of Chemistry, University of Washington, Seattle, Washington 98195, United States; Pacific Northwest National Laboratory, Richland, Washington 99354, United States; [orcid.org/0000-0001-7341-6240](https://orcid.org/0000-0001-7341-6240); Email: [xsli@uw.edu](mailto:xsli@uw.edu)

## Authors

Tianyuan Zhang – Department of Chemistry, University of Washington, Seattle, Washington 98195, United States

Xiaolin Liu – Department of Chemistry, University of Washington, Seattle, Washington 98195, United States

Edward F. Valeev – Department of Chemistry, Virginia Tech, Blacksburg, Virginia 24061, United States; [orcid.org/0000-0001-9923-6256](https://orcid.org/0000-0001-9923-6256)

Complete contact information is available at:  
<https://pubs.acs.org/10.1021/acs.jpca.1c02317>

## Notes

The authors declare no competing financial interest.

## ■ ACKNOWLEDGMENTS

T.Z. thanks Dr. Folkestad and Dr. Kjønsstad for valuable discussion on the span-factor algorithm. The development of the efficient relativistic method is supported by the U.S. Department of Energy in the Heavy-Element Chemistry Program (grant no. DE-SC0021100 to X.L.). The development of the Chronus Quantum open-source software package is supported by the National Science Foundation (OAC-1663636). X.L. also acknowledges support for the low-scaling method development from the Computational Chemical Sciences (CCS) Program of the U.S. Department of Energy, Office of Science, Basic Energy Sciences, Chemical Sciences, Geosciences, and Biosciences Division in the Center for Scalable and Predictive methods for Excitations and Correlated phenomena (SPEC) at the Pacific Northwest National Laboratory.

## ■ REFERENCES

- (1) Beebe, N. H. F.; Linderberg, J. Simplifications in the Generation and Transformation of Two-Electron Integrals in Molecular Calculations. *Int. J. Quantum Chem.* **1977**, *12*, 683–705.
- (2) Røeggen, I.; Wisloff-Nilsen, E. On the Beebe-Linderberg Two-Electron Integral Approximation. *Chem. Phys. Lett.* **1986**, *132*, 154–160.
- (3) Koch, H.; Sánchez de Merás, A.; Pedersen, T. B. Reduced Scaling in Electronic Structure Calculations Using Cholesky Decompositions. *J. Chem. Phys.* **2003**, *118*, 9481–9484.
- (4) Boman, L.; Koch, H.; Sánchez de Merás, A. Method Specific Cholesky Decomposition: Coulomb and Exchange energies. *J. Chem. Phys.* **2008**, *129*, 134107.
- (5) Aquilante, F.; Lindh, R.; Bondo Pedersen, T. Unbiased Auxiliary Basis Sets for Accurate Two-Electron Integral approximations. *J. Chem. Phys.* **2007**, *127*, 114107.
- (6) Aquilante, F.; Gagliardi, L.; Pedersen, T. B.; Lindh, R. Atomic Cholesky Decompositions: A Route to Unbiased Auxiliary Basis Sets for Density Fitting Approximation with Tunable Accuracy and Efficiency. *J. Chem. Phys.* **2009**, *130*, 154107.
- (7) Whitten, J. L. Coulombic Potential Energy Integrals and Approximations. *J. Chem. Phys.* **1973**, *58*, 4496–4501.
- (8) Dunlap, B. I.; Connolly, J. W. D.; Sabin, J. R. On Some Approximations in Applications of  $X\alpha$  Theory. *J. Chem. Phys.* **1979**, *71*, 3396–3402.
- (9) Kendall, R. A.; Früchtel, H. A. The Impact of the Resolution of the Identity Approximate Integral Method on Modern Ab Initio Algorithm Development. *Theor. Chem. Acc.* **1997**, *97*, 158–163.
- (10) Aquilante, F.; Pedersen, T. B.; Lindh, R.; Roos, B. O.; Sánchez de Merás, A.; Koch, H. Accurate Ab Initio Density Fitting for Multiconfigurational Self-Consistent Field Methods. *J. Chem. Phys.* **2008**, *129*, 024113.
- (11) Sherrill, C. D. Frontiers in Electronic Structure Theory. *J. Chem. Phys.* **2010**, *132*, 110902.
- (12) Hohenstein, E. G.; Sherrill, C. D. Density Fitting and Cholesky Decomposition Approximations in Symmetry-Adapted Perturbation Theory: Implementation and Application to Probe the Nature of  $\pi$ - $\pi$  Interactions in Linear Acenes. *J. Chem. Phys.* **2010**, *132*, 184111.
- (13) Bozkaya, U.; Sherrill, C. D. Analytic Energy Gradients for the Coupled-Cluster Singles and Doubles Method with the Density-Fitting Approximation. *J. Chem. Phys.* **2016**, *144*, 174103.
- (14) Epifanovsky, E.; Zuev, D.; Feng, X.; Khistyayev, K.; Shao, Y.; Krylov, A. I. General Implementation of the Resolution-of-the-Identity and Cholesky Representations of Electron Repulsion Integrals within Coupled-Cluster and Equation-of-Motion Methods: Theory and Benchmarks. *J. Chem. Phys.* **2013**, *139*, 134105.
- (15) Fosso-Tande, J.; Nguyen, T.-S.; Gidofalvi, G.; DePrince, A. E. Large-Scale Variational Two-Electron Reduced-Density-Matrix-Driven Complete Active Space Self-Consistent Field Methods. *J. Chem. Theory Comput.* **2016**, *12*, 2260–2271.
- (16) Freitag, L.; Knecht, S.; Angeli, C.; Reiher, M. Multireference Perturbation Theory with Cholesky Decomposition for the Density Matrix Renormalization Group. *J. Chem. Theory Comput.* **2017**, *13*, 451–459.
- (17) Motta, M.; Shee, J.; Zhang, S.; Chan, G. K.-L. Efficient Ab Initio Auxiliary-Field Quantum Monte Carlo Calculations in Gaussian Bases via Low-Rank Tensor Decomposition. *J. Chem. Theory Comput.* **2019**, *15*, 3510–3521.
- (18) Hannon, K. P.; Li, C.; Evangelista, F. A. An Integral-Factorized Implementation of the Driven Similarity Renormalization Group Second-Order Multireference Perturbation Theory. *J. Chem. Phys.* **2016**, *144*, 204111.
- (19) Zhang, T.; Li, C.; Evangelista, F. A. Improving the Efficiency of the Multireference Driven Similarity Renormalization Group via Sequential Transformation, Density Fitting, and the Noninteracting Virtual Orbital Approximation. *J. Chem. Theory Comput.* **2019**, *15*, 4399–4414.
- (20) Bozkaya, U. Efficient Implementation of the Second-Order Quasidegenerate Perturbation Theory with Density-Fitting and Cholesky Decomposition Approximations: Is It Possible To Use Hartree–Fock Orbitals for a Multiconfigurational Perturbation Theory? *J. Chem. Theory Comput.* **2019**, *15*, 4415–4429.
- (21) Lesiuk, M. Implementation of the Coupled-Cluster Method with Single, Double, and Triple Excitations using Tensor Decompositions. *J. Chem. Theory Comput.* **2020**, *16*, 453–467.
- (22) Weigend, F.; Kattannek, M.; Ahlrichs, R. Approximated Electron Repulsion Integrals: Cholesky Decomposition Versus Resolution of the Identity Methods. *J. Chem. Phys.* **2009**, *130*, 164106.
- (23) Aquilante, F.; Boman, L.; Boström, J.; Koch, H.; Lindh, R.; de Merás, A. S.; Pedersen, T. B. In *Linear-Scaling Techniques in Computational Chemistry and Physics: Methods and Applications*; Zalesny, R., Papadopoulos, M. G., Mezey, P. G., Leszczynski, J., Eds.; Springer Netherlands: Dordrecht, 2011; pp 301–343.
- (24) Folkestad, S. D.; Kjønsstad, E. F.; Koch, H. An Efficient Algorithm for Cholesky Decomposition of Electron Repulsion Integrals. *J. Chem. Phys.* **2019**, *150*, 194112.
- (25) Williams-Young, D. B.; Petrone, A.; Sun, S.; Stetina, T. F.; Lestrang, P.; Hoyer, C. E.; Nascimento, D. R.; Koulias, L.; Wildman, A.; Kasper, J.; et al. The Chronus Quantum (ChronusQ) Software Package. *Wiley Interdiscip. Rev.: Comput. Mol. Sci.* **2020**, *10*, No. e1436.
- (26) Valeev, E. F. Libint: A Library for the Evaluation of Molecular Integrals of Many-body Operators over Gaussian Functions. <http://libint.valeev.net/version2.7.0-beta.6> (accessed April 20, 2021).

- (27) Hehre, W. J.; Stewart, R. F.; Pople, J. A. Self-Consistent Molecular-Orbital Methods. I. Use of Gaussian Expansions of Slater-Type Atomic Orbitals. *J. Chem. Phys.* **1969**, *51*, 2657–2664.
- (28) Dunning, T. H. Gaussian Basis Sets for Use in Correlated Molecular Calculations. I. The Atoms Boron Through Neon and Hydrogen. *J. Chem. Phys.* **1989**, *90*, 1007–1023.
- (29) Becke, A. D. Density-functional Thermochemistry. III. The Role of Exact Exchange. *J. Chem. Phys.* **1993**, *98*, 5648–5652.
- (30) Lee, C.; Yang, W.; Parr, R. G. Development of the Colle-Salvetti Correlation-Energy Formula into a Functional of the Electron Density. *Phys. Rev. B: Condens. Matter Mater. Phys.* **1988**, *37*, 785–789.
- (31) Miehlich, B.; Savin, A.; Stoll, H.; Preuss, H. Results Obtained With the Correlation Energy Density Functionals of Becke and Lee, Yang and Parr. *Chem. Phys. Lett.* **1989**, *157*, 200–206.
- (32) Martins, L. S. C.; Jorge, F. E.; Machado, S. F. All-Electron Segmented Contraction Basis Sets of Triple Zeta Valence Quality for the Fifth-Row Elements. *Mol. Phys.* **2015**, *113*, 3578–3586.
- (33) Hess, B. A. Relativistic Electronic-Structure Calculations Employing a Two-Component No-Pair Formalism with External-Field Projection Operators. *Phys. Rev. A: At., Mol., Opt. Phys.* **1986**, *33*, 3742–3748.
- (34) Liu, W.; Peng, D. Infinite-Order Quasirelativistic Density Functional Method Based on the Exact Matrix Quasirelativistic Theory. *J. Chem. Phys.* **2006**, *125*, 044102.
- (35) Liu, W.; Peng, D. Exact Two-component Hamiltonians Revisited. *J. Chem. Phys.* **2009**, *131*, 031104.
- (36) Kutzlenigg, W.; Liu, W. Quasirelativistic Theory Equivalent to Fully Relativistic Theory. *J. Chem. Phys.* **2005**, *123*, 241102.
- (37) Liu, W. Ideas of Relativistic Quantum Chemistry. *Mol. Phys.* **2010**, *108*, 1679–1706.
- (38) Ilias, M.; Saue, T. An Infinite-Order Relativistic Hamiltonian by a Simple One-Step Transformation. *J. Chem. Phys.* **2007**, *126*, 064102.
- (39) Saue, T. Relativistic Hamiltonians for Chemistry: A Primer. *ChemPhysChem* **2011**, *12*, 3077–3094.
- (40) Kasper, J. M.; Lestranger, P. J.; Stetina, T. F.; Li, X. Modeling  $L_{2,3}$ -Edge X-ray Absorption Spectroscopy with Real-Time Exact Two-Component Relativistic Time-Dependent Density Functional Theory. *J. Chem. Theory Comput.* **2018**, *14*, 1998–2006.
- (41) Zhang, T.; Kasper, J. M.; Li, X. In *Annual Reports in Computational Chemistry*; Dixon, D. A., Ed.; Elsevier: Amsterdam, 2020; Vol. 16; pp 17–37.
- (42) Perdew, J. P.; Burke, K.; Ernzerhof, M. Generalized Gradient Approximation Made Simple. *Phys. Rev. Lett.* **1996**, *77*, 3865–3868.
- (43) Perdew, J. P.; Burke, K.; Ernzerhof, M. Errata: Generalized Gradient Approximation Made Simple [Phys. Rev. Lett. 77, 3865 (1996)]. *Phys. Rev. Lett.* **1997**, *78*, 1396.
- (44) Adamo, C.; Barone, V. Toward Reliable Density Functional Methods Without Adjustable Parameters: The PBE0 Model. *J. Chem. Phys.* **1999**, *110*, 6158–6170.
- (45) Ditchfield, R.; Hehre, W. J.; Pople, J. A. Self-Consistent Molecular-Orbital Methods. IX. An Extended Gaussian-Type Basis for Molecular-Orbital Studies of Organic Molecules. *J. Chem. Phys.* **1971**, *54*, 724–728.
- (46) Hehre, W. J.; Ditchfield, R.; Pople, J. A. Self-Consistent Molecular Orbital Methods. XII. Further Extensions of Gaussian-Type Basis Sets for Use in Molecular Orbital Studies of Organic Molecules. *J. Chem. Phys.* **1972**, *56*, 2257–2261.
- (47) Hariharan, P. C.; Pople, J. A. The Influence of Polarization Functions on Molecular Orbital Hydrogenation Energies. *Theor. Chem. Acc.* **1973**, *28*, 213–222.
- (48) Canal Neto, A.; Jorge, F. E. All-electron Double Zeta Basis Sets for the Most Fifth-Row Atoms: Application in DFT Spectroscopic Constant Calculations. *Chem. Phys. Lett.* **2013**, *582*, 158–162.
- (49) Noro, T.; Sekiya, M.; Koga, T. Sapporo-(DKH3)-nZP (n = D, T, Q) Sets for the Sixth Period s-, d-, and p-Block Atoms. *Theor. Chem. Acc.* **2013**, *132*, 1363.